Int. J. Electrochem. Sci., 16 **(2021)** Article Number: 211111, doi: 10.20964/2021.11.45

International Journal of
ELECTROCHEMICAL
SCIENCE
www.electrochemsci.org

Electrochemical Determination of Chemical Oxygen Demand in Mixed Organic Solution by Al/SnO_2-TiO_2 Electrode

Xiaojiao Li [1, 2], *Yan Shang* [3], *Carlos Fernandez* [4], *Tingting Pei* [1], *Linshan Wang* [1,*]

[1] College of Sciences, Northeastern University, Shenyang 110819, P.R. China.
[2] School of Materials Science and Engineering, Northeastern University, Shenyang 110819, P.R. China.
[3] Chemical Experiment Center, Department of Basic Science, JilinJianzhu University, Changchun 130118, P.R. China.
[4] School of Pharmacy and Life Sciences, Robert Gordon University, AB107GJ, Aberdeen, UK.
[*]E-mail: lswang@mail.neu.edu.cn

Received: 9 August 2021 / *Accepted:* 10 September 2021 / *Published:* 10 October 2021

Chemical oxygen demand (COD) is one of the most significant parameters in water-quality analysis, such as wastewater effluent monitoring. However, COD determination faces challenges of long measuring time and the use of toxic substances. In this work, an Al/SnO_2-TiO_2 composite film electrode was prepared using the sol-gel method and dip-coating method for electrochemical determination of COD. The electrocatalytic reaction kinetics of the different organic substances on the electrode was studied in a three-electrode system. It was observed that the electrocatalytic reactions of all tested organic compounds on the Al/SnO_2-TiO_2 electrode fitted the first-order kinetics. Based on the reaction rate constants at different temperatures, the activation energies for electrocatalytic oxidations of methylene blue and rhodamine B were 9.92 kJ/mol and 14.7 kJ/mol, respectively. It was confirmed that dynamic behaviors of different organic substances on the electrode surface were different from each other. In addition, seven single-component organic solutions, four two-component organic solutions, and three three-component organic solutions were selected as the target standard solutions for the COD measurement experiments. Initial working currents measured by chronocoulometry were taken as the index of the value of COD of the target solutions within the operating voltage range of 1.5~3.5 V (vs. SCE). In the range of 20~100 mg/L, COD values of either single-component or multiple-component solutions were linearly related to the initial working currents. For solutions composed of different organic compounds with the identical COD concentration, each of their initial working currents was different from the others and increased with the working voltage. It could be concluded that the initial working currents measured by chronocoulometry was depended on COD concentration, applied voltage, as well as the composition of the tested solutions. By comparing the COD measurement results, using potassium hydrogen phthalate solution as the simulated wastewater, of the presented method with those of the standard potassium dichromate method, the accuracy and reproducibility of this method had also been approved. Therefore, we report a simple, rapid, and environmentally friendly COD determination method using an Al/SnO_2-TiO_2 electrode, which is feasible for single- and multiple-component organic solutions.

Keywords: Chemical oxygen demand; Electrochemical method; Multi-component solution; Al/SnO_2-TiO_2 electrode

1. INTRODUCTION

Chemical oxygen demand (COD) is one of the most widely used parameters of water-quality analysis [1]. For industrial sewage and domestic wastewater, the traditional COD method is currently used for the COD detecting or monitoring, namely the potassium dichromate method. The potassium dichromate method measures COD by refluxing the sample for 2 hours under strong-acid conditions with the addition of silver salt as a catalyst. After that, ferrous ammonium sulfate is used as a titration reagent. The amount of ferrous ammonium sulfate consumed is obtained from titration, and finally, the concentration of oxygen consumed is calculated [2, 3]. In addition, the chloride ions in the solution are likely to react with silver sulfate to produce precipitation, which leads to a deviation in the measurement results. Therefore, mercury sulfate is used to form a complex for eliminating the interference of chloride ions. Despite the advantages of accurate results, the potassium dichromate method, as a standard method for COD analysis and detection, also has obvious shortcomings, such as complicated operation steps, long experiment time, secondary pollution, difficulty to automate monitoring. [2-4].

To overcome the shortcomings of the potassium dichromate method, researchers have done lots of work to develop fast and environmentally friendly COD analysis and detection methods, which are commonly divided into three categories [1, 5-7]. The first category is designed on the basis of the traditional potassium dichromate method [8, 9]. It is improved by shortening the analysis time, reducing the consumption of chemical reagents, and replacing the titration method with spectrophotometry. Jirka [8] et al. developed a semi-automatic measurement method based on the traditional potassium dichromate method. The method used closed glass digestion instead of reflux and measured Cr^{3+} by spectrophotometry instead of measuring Cr(VI) by titration. It could digest water samples in batches; the digestion time reduced from 120 min to 15 min; the consumption of chemical reagents is 5% of the traditional method; the measurement accuracy also improved. However, secondary pollution was fundamentally unavoided in this type of method. The second category directly or indirectly determines COD using photometry, such as ultraviolet-visible spectrophotometry[5, 10, 11]. Matsche [12] reported that the absorbance of wastewater at 260 nm is linearly related to the COD value of wastewater. The significant merits of the spectrophotometric method for measuring COD consist in being fast and needing no chemical additives that may bring out secondary pollution. However, the result in this type of method is easily affected by the turbidity and composition of the water sample, so the measurement accuracy is difficult to guarantee. The third category is upon the electrocatalytic oxidation method, which can be divided into three types, including electrochemical (EC) [13-21], photoelectrochemical (PEC) [22-24], and photocatalytic (PC) [25-29].

The PC method is directly oxidizing organic matter under chemical catalyst and ultraviolet light. The principle of this method is based on the reduction of dissolved oxygen concentration in water body is proportional to COD concentration. The main disadvantages of the PC method are low photocatalytic efficiency and poor reproducibility [25-29]. Compared with the PC method, the oxidation capacity and

efficiency of the PEC method have been improved. But the use of illumination equipment has increased the complexity and manufacturing cost of the analysis and detection equipment. Because TiO_2 has excellent photoelectrochemical properties, the PEC method usually uses TiO_2 as one of the electrode compositions. However, the preparation process is very complicated, and the cost is high. There are many kinds of electrodes for EC method (such as Cu [3, 30], CoO, Pt/PbO_2 [31, 32], glassy carbon/NiCu, Ti/Sb-SnO_2/PbO_2 [16], boron-doped diamond [33]). However, there are few reports on the use of electrodes containing TiO_2 for COD determination by the EC method [2] (Ti/TiO_2 [24]). Compared with other electrodes, the electrodes with TiO_2 are more promising for the EC method because of the superior oxidative abilities of TiO_2, low cost, non-toxic nature, short analysis time, etc. [34-38]. In addition, it also has a high-efficiency photoelectric conversion performance, which can be applied in the utilization of solar energy. Therefore, for the EC method, the electrode with TiO_2, as a promising COD analysis and detection technology, needs to develop in the research of electrode preparation and electrode reaction mechanism.

To deeply study the research, we had prepared an Al/SnO_2-TiO_2 electrode by sol-gel method and dip-coating method. The preparation and composition of the electrode, the electrode reaction kinetics of different organic matters on the electrode surface, and its application in COD determination of single- and multi-component organic solutions are described in detail below.

2. MATERIALS AND METHODS

2.1 Materials

Aluminum sheet (Al sheet), tetrabutyl titanate, stannic chloride, sulfuric acid (H_2SO_4, 98 wt%), phenol (PhOH), aniline (An), propanedioic acid (PDA), and sodium acetate (NaAc) were purchased from Sinopharm Chemical Reagent Co., Ltd., China. Sodium sulfate (Na_2SO_4), methyl orange (MO), methylene blue (MB), glucose (GLc), and rhodamine B (RhB) were brought from Damao Chemical Reagent Factory, Tianjin, China. Oxalic acid, acetic acid (HAc), potassium hydrogen phthalate (KHP), and anhydrous ethanol were from Shenyang Chemical Reagent Factory, Shenyang, China. Silver sulfate (Ag_2SO_4) and potassium dichromate ($K_2Cr_2O_7$) were purchased from Shenyang Xinxing Reagent Factory, Shenyang, China. Moreover, distilled water was used for all purposes.

2.2 Preparation of an Al/SnO_2-TiO_2 electrode

The Al/SnO_2-TiO_2 composite film electrode was coated with SnO_2-TiO_2 film on an Al matrix by sol-gel method combined with dip-coating. The Al sheet was polished with 400#, 800#, and 1500# sandpaper in order, to remove oxide from the surface and polish smooth. Then it was rinsed with deionized water, dry, and reserve. The sample was immersed in 5 wt.% Na_2CO_3 solution and ultrasonic-cleaned for 20~30 min to remove oil stains. Then it was placed in 10% oxalic acid solution and heated in a water bath at 90 ℃ for 2~3 h for acid etching. The pretreated Al sheet was rinsed with deionized water and stored in a 1% oxalic acid solution.

A tetrabutyl titanate solution was prepared by dissolving 34 mL tetrabutyl titanate and 23 mL acetic acid in 100 mL anhydrous ethanol under constant stirring for 30 min. A homogeneous tin source solution was obtained by dissolving 22 mL stannic chloride aqueous solution (0.1 mol/L) in 50 mL ethanol. The tin source solution was slowly added into the tetrabutyl titanate solution. The mixed solution was heated at 60 ℃ in a water bath for 30 min to finally achieve a light-yellow transparent colloid with 4 wt% tin. The gel was evenly coated on the treated Al matrix three time by dip-coating [39, 40]. After natural drying, it was calcined at 500 ℃ for 1 h in a muffle furnace and then cooled naturally.

2.3 Instrumental characterization and electrochemical measurement

A field emission scanning electron microscope （FE-SEM, SSX- 550, Shimazu Co., Japan） was used to observe the morphological information of the electrode surface. The crystal structure of the electrode surface coating was measured with the X-ray diffractometer (XRD, Empyrean, PANalytical Co., Netherlands) using Cu target. The scanning range was 20°~80° under Ni filter tube voltage 45 kV and tube current 100 mA. The test results were processed by MDI Jade 6.0 analysis software. A double beam ultraviolet-visible spectrophotometer (UV-vis, TU-1901, Beijing Puxi General Instrument Co., Ltd., China) was used to analyze the solution absorbance. The absorbances of methylene blue and rhodamine B were analyzed by UV-vis at 664 and 230 nm wavelengths, respectively. The degradation rate (η, %) and activation energy (Ea, kJ/mol) of the detected solution were calculated by the following Equation 1 and the Arrhenius formula (Equation 2), respectively.

$$\eta\ (\%)=\frac{A_0-A_t}{A_0} \tag{1}$$

$$\ln k=-\frac{E_a}{RT}+\ln A \tag{2}$$

Herein, A_0 and A_t are the absorbance of the initial standard organic solution and the degraded organic solution at a degradation time t [37, 41]. Moreover, k is the reaction rate constant, T stands for the absolute temperature (K), R is the molar gas constant (8.314 J/mol·K), and A represents the pre-exponential factor.

Chronocoulometry was applied to measure the anodic oxidation current of the standard organic solution in the three-electrode system on an electrochemical workstation (CS350, Wuhan Kester Instrument Co., Ltd., China). The prepared Al/SnO_2-TiO_2 film electrode, a porous graphite electrode, and a standard calomel electrode (SCE) were employed as the working electrode, the auxiliary electrode and the reference electrode, respectively. A 0.1 mol/L sodium sulfate solution was used as a supporting electrolyte. The standard solutions for detection were a series of organic solutions with known COD concentrations, prepared by dissolving quantitative target organic matters (such as rhodamine B, phenol, and aniline) into the supporting electrolyte [42].

The same three-electrode system was employed for electrocatalytic degradation, electrolysis kinetics and COD determination by Al/SnO_2-TiO_2 film electrode. For studying on kinetic mechanism of electrolysis, the target organic solutions of methylene blue and rhodamine B were of 50 mg/L COD concentration. For COD determination experiments, the COD value of the target organic solution ranged from 20 mg/L to 100 mg/L. The relationship of COD vs. ΔI, the current was detected in the three-

electrode system under different voltages (1.5 V, 2.0 V, 2.5 V, 3.0 V, and 3.5 V) for single-, two-, and three-component solutions. The single-component solutions included phenol (PhOH), propanedioic acid (PDA), sodium acetate (NaAc), potassium hydrogen phthalate (KHP), methylene blue (MB), methyl orange (MO), and glucose (GLc). The two-component solutions in the COD ratio of 1:1 included aniline/rhodamine B (An/RhB), potassium hydrogen phthalate, phenol (KHP/PhOH), sodium acetate, glucose (NaAc/GLc), and methylene blue/methyl orange (MB/MO). The three-component solutions in the COD ratio of 1:1:1 included aniline/sodium acetate/glucose (An/NaAc/GLc), potassium hydrogen phthalate/rhodamine B/methyl orange (KHP/RhB/MO), and methylene blue/phenol/acetic acid (MB/PhOH/HAc).

3. RESULTS AND DISCUSSION

3.1 Morphology characterization

Figure 1 shows the SEM diagram of the Al-based SnO_2-TiO_2 electrode prepared by dip-coating with three layers. There are many bulges and grooves on the surface, which is conducive to increasing the specific surface area of the electrode surface. The electrode can provide lots of active sites, thereby enhancing the adsorption capacity of organic molecules and naturally forming Schottky-type contacts [43]. The high surface area of the prepared Al/SnO_2-TiO_2 electrode lays a foundation for the catalytic performance of the electrode [44].

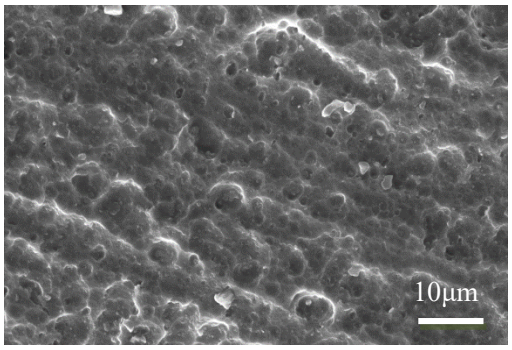

Figure 1. SEM image of the Al/SnO_2-TiO_2 film electrode

3.2 Composition analysis

In order to further study the material of the composite electrode prepared by the sol-gel method combined with dip-coating, the electrode was characterized by XRD. Figure 2 shows the XRD pattern of the Al-based SnO_2-TiO_2 electrode. The diffraction peaks of Al, rutile TiO_2, anatase TiO_2, and SnO_2 were displayed, according to the PDF card No. 04-0787 of Al, No. 73-1765 of the rutile phase TiO_2, No. 21-1272 of the anatase phase, and No. 41-1445 of the cassiterite phase SnO_2 [45, 46]. The strong peak at 2θ=44.09° exhibited that the crystal type of TiO_2 film electrode sintered at 500℃ mainly exists in

rutile type. It was ascribed that after calcining about 330~650 ℃, rutile phase and anatase phase coexist in crystal of TiO_2. Generally, after calcining at 500~700 ℃, the rutile TiO_2 was achieved with the highest catalytic activity compared with the amorphous and anatase TiO_2 [44, 47, 48]. In addition, the presence of Al was due to the hollow holes in the oxide layer, through which the X-ray could contact the Al matrix, reflecting its crystal characteristics. Therefore, the XRD pattern indicated that the composition of the oxide layer of the composite film electrode was mainly rutile TiO_2 and cassiterite SnO_2.

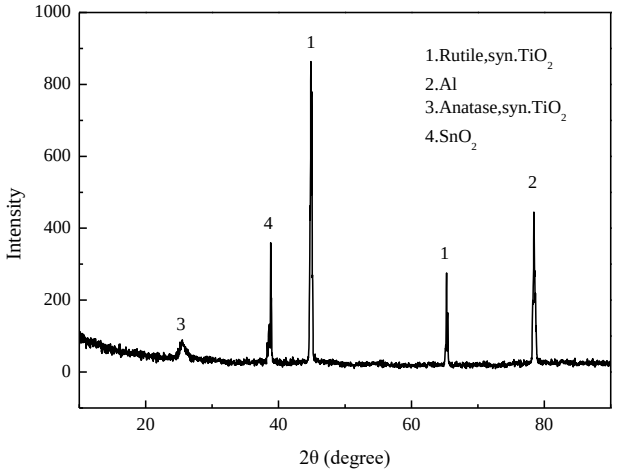

Figure 2. XRD pattern of the Al/SnO_2-TiO_2 film electrode

3.3 Chronocoulometry study

The work current was determined by chronocoulometry. The chronocoulometric curves in Figure 3 were determined in KHP solutions with different concentrations of 0~500 mg/L containing 0.1 mol/L Na_2SO_4. Figure 3 shows the charge in Coulombs as a function of time. The slopes were the values of the currents. The net current (ΔI) was the difference between the work current of the sample and that of the blank. The higher the concentration of the solution applied, the higher the net current measured.

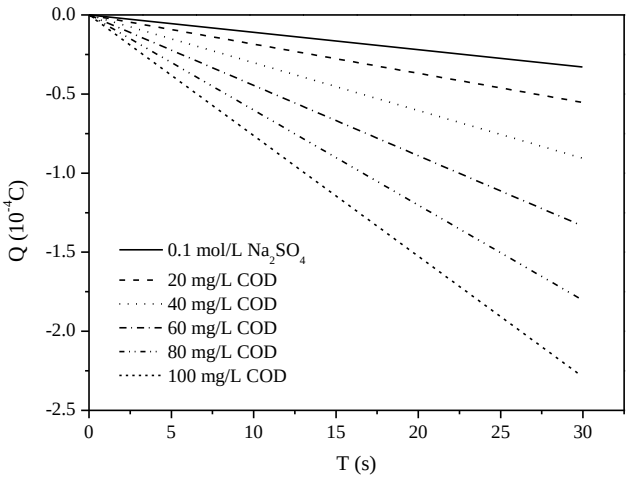

Figure 3. Chronocoulometric curves of KHP solutions with different concentrations

3.4 Electrocatalytic degradation and electrolysis kinetics

At different temperatures of 298~328 K, the anodic oxidation currents of organic solutions (methylene blue and rhodamine B) with an initial COD concentration of 50 mg/L were investigated in the three-electrode system. The relationship between degradation rate and reaction time in electrocatalytic degradation at different temperatures was studied (Figure 4), and the relevant kinetic parameters were obtained (Table 4).

In Figure 4, the degradation rate of organic matter increased sharply within 60 min, then the increase of degradation rate slowed down. The degradation rate of organic compounds (methylene blue and rhodamine B [49]) increased with the rise of temperature. It was mainly caused by the enhanced diffusion of organic molecules toward the electrode and the increase in the catalytic activity of the process with the temperature rise-up [50-52]. It increased the direct catalytic reaction capacity of the electrode surface and generated more hydroxyl radical ·OH, thereby improving the electrocatalytic activity of the indirect reaction [50-52] . At 328 K, the degradation rate for each target organic solution (methylene blue and rhodamine B) was the highest, reaching 89.3% and 97.3% at 100 min, respectively. It indicated that the degradation behavior of different organics on the prepared Al/SnO_2-TiO_2 electrode surface was different, which meant that the degradation rate was dependent on the type of organics.

In Figure 5, the $\ln(C_0/C_t)$ for each target organic matter was increased linearly with the reaction time t. In addition, $\ln(C_0/C_t)$-t curves at different temperatures had good linearity, according to the correlation coefficients (R^2>0.99) shown in Table 1. Therefore, the electrochemical degradation processes of methylene blue and rhodamine B followed quasi-first-order kinetics. The ·OH was stably produced under the electrocatalytic reaction of the electrode, and the process was a free radical reaction process [13, 53]. The reaction rate constants at different temperatures in Table 1 were employed to obtain the figure of lnk~1/T (Figure 6). The reaction rate constant k at different temperatures (Table 1) was used to obtain the figure of lnk~1/T (Figure 6). According to the Arrhenius formula, the activation energies of methylene blue and rhodamine B on the electrode reaction were 9.92 kJ/mol and 14.7 kJ/mol, respectively. According to the general chemical reaction with 60~250 kJ/mol activation energy, the much lower activation energies of methylene blue and rhodamine B on the electrode reaction indicated that their electrochemical degradation was very easy to proceed. The electrocatalytic degradation of rhodamine B required relatively higher energy than that of methylene blue. It confirmed that the organic compounds degraded with different degradation efficiency on the prepared Al/SnO_2-TiO_2 electrode. It may be because that electrochemical degradation process was affected by functional groups of organics which include the promoting groups (such as hydroxyl group and amine group) and inhibitory groups (such as carboxyl groups and methyl group) [54-56]. Methylene blue and rhodamine B belong to polycyclic aromatic hydrocarbons. For the aromatic ring organics with promoting groups and inhibiting groups, the degradability of the dye depends on the synergistic effect of the groups. In contrast to methylene blue, the molecular structure of RhB has inhibitory carboxyl groups (-COOH), which inhibits the electrocatalytic degradation of -OH. Therefore, the degradation reaction of methylene blue was easier to proceed with, and the electrochemical reactivity relationship of both organics was methylene blue>rhodamine B.

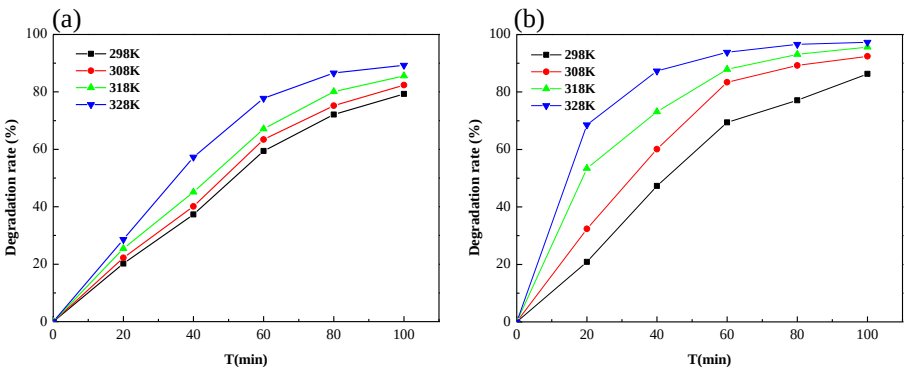

Figure 4. The degradation rate of methylene blue (a) and rhodamine B (b) with reaction time at different temperatures at the voltages of 5 V. The target organic solutions were of 50 mg/L COD concentration.

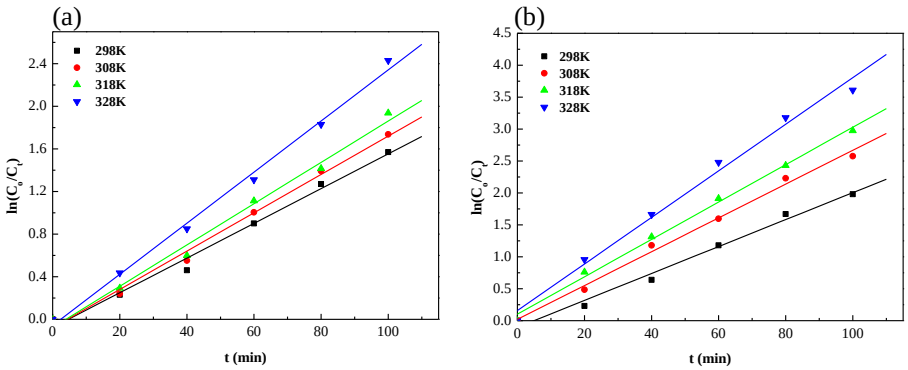

Figure 5. The curves of the reaction time vs. the $\ln(C_0/C_t)$ of methylene blue (a) and rhodamine B (b) at different temperatures. C_0 and C_t is the initial organic concentration and the organic concentration at the reaction time.

Table 1. Kinetic equations and correlation coefficients of methylene blue and rhodamine B at different temperatures

Organics	Temperature (℃)	Linear regression equation (C_t, mol/L; t, min)	Kinetic constant k (min^{-1})	R^2
Methylene blue	25	$C_t=50e^{-0.0163t}$	0.0163	0.994
	35	$C_t=50e^{-0.0179t}$	0.0179	0.996
	45	$C_t=50e^{-0.0193t}$	0.0193	0.995
	55	$C_t=50e^{-0.0241t}$	0.0241	0.998
Rhodamine B	25	$C_t=50e^{-0.021t}$	0.021	0.994
	35	$C_t=50e^{-0.026t}$	0.026	0.996
	45	$C_t=50e^{-0.029t}$	0.029	0.998
	55	$C_t=50e^{-0.036t}$	0.036	0.995

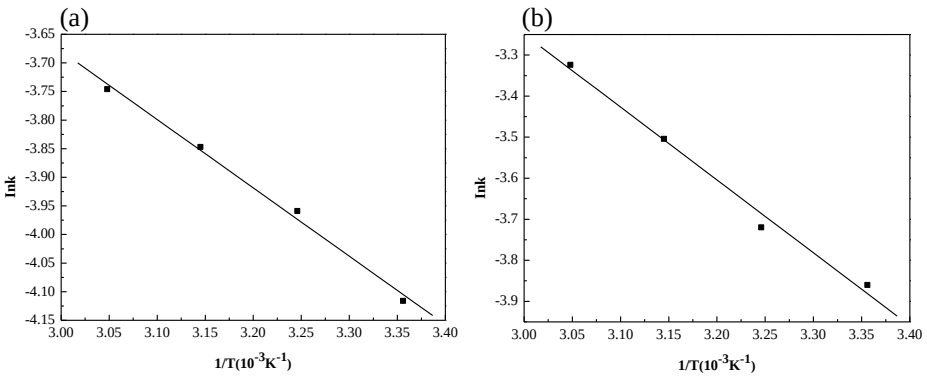

Figure 6. The linear curves of lnk vs. 1/T for methylene blue (a) and rhodamine B (b)

In Figure 4, the degradation rate of methylene blue and rhodamine B increased with the rise of temperature from 298 to 328 K. Furthermore, the kinetic behavior of the target organic matter on the Al/SnO_2-TiO_2 composite electrode surface was studied by analyzing the relationship between the concentration of organic solution and reaction time (Figure 5 and Table1). The electrocatalytic reactions of methylene blue and rhodamine B were free radical processes, conformed to the first order kinetic reaction. According to the reaction rate constant k at different temperatures, the activation energies of methylene blue and rhodamine B were calculated from the slopes to be 9.92 kJ/mol and 14.7 kJ/mol, respectively. Under the same catalytic conditions, different kinetic parameters were obtained for different organic substances, and the kinetic behavior of the organic substances on the electrode surface was distinct. The electrochemical reactivity relationship of two organics on the electrode surface was methylene blue>rhodamine B, owing to the synergistic effect of the functional groups.

Due to the low activation energies of both organics, the Al/SnO_2-TiO_2 electrode exhibited high catalytic degradation ability for the representative organics. The uneven surface structure of the prepared electrode provided a large number of attachment and adsorption sites for the organics, improving the electrocatalytic degradation rate of the electrode. It was also ascribed to the increased catalytic activity of the catalyst as the temperature increased.

3.5 COD determination by Al/SnO_2-TiO_2 film electrode

3.5.1 COD determination of single-component solution

In this work, the current values were measured with chronocoulometry under different voltages for PhOH, PDA, NaAc, KHP, MB, MO, and GLc single-component standard solutions with a COD concentration gradient of 20~100 mg/L. Figure 7 shows the relationship between COD and net current ΔI of PhOH, PDA, NaAc, KHP, MB, MO, and GLc under different voltages of 1.5~3.5 V (vs. SCE) [18]. It revealed that the response current increased gradually with COD concentration and presented good linear relationships. It was ascribed to more organic pollutants oxidized by the electrode and the generation of more electrons, resulting in a higher current value [17, 57]. At the same voltage, the net current from the electrode had the largest response to MB and the lowest response to PDA in Figure 7.

Thus, the linear COD vs. ΔI relationship of the different organic compounds was different under the same conditions. As shown in Figure 7, the electrochemical reactivity relationship of the target organic matters was PDA<NaAc<PhOH<GLc<MO<KHP<MB. Therefore, the net current was affected not only by the COD concentration but also by the type of organic matter. In addition, the ranges of the net current of MB in 100 min of electrolysis are 5.8~12.8 μA, 20.8~55.2 μA, 46.9~113.3 μA, 89.5~194.2 μA, 155.6~362.7 μA at the voltages of 1.5 V, 2.0 V, 2.5 V, 3.0 V, and 3.5 V, respectively. It indicated that with the increase of voltage, the net current values of the target organic solutions increased correspondingly.

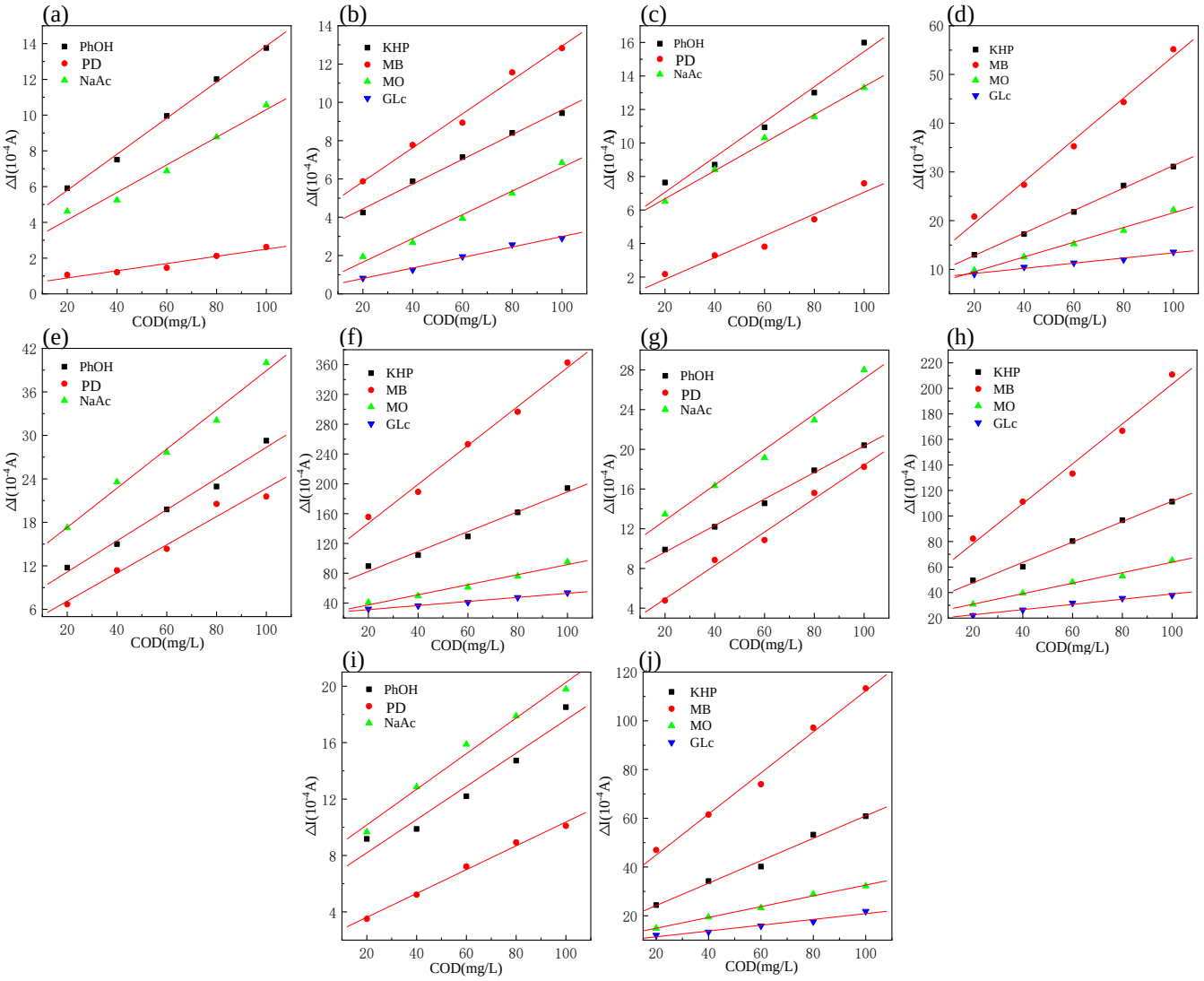

Figure 7. The linear curves of the net current (ΔI) vs. the COD concentration of the single-component organic solutions at the voltages of 1.5 V (a, b), 2.0 V (c, d), 2.5 V (e, f), 3.0 V (g, h), and 3.5 V (i, j), measured by the prepared Al/SnO_2-TiO_2 electrode. The PhOH, PDA, NaAc, KHP, MB, MO, and GLc represent phenol, propanedioic acid, sodium acetate, potassium hydrogen phthalate, methylene blue, methyl orange, and glucose, respectively.

Table 2. Linear regression equations of the net current (ΔI) and the COD concentration for the target organic solutions

Voltage (V·vs. SCE)	1.5		2.0		2.5	
	Linear regression equation (ΔI, μA; COD, mg/L)	R^2	Linear regression equation (ΔI, μA; COD, mg/L)	R^2	Linear regression equation (ΔI, μA; COD, mg/L)	R^2
PhOH	ΔI=0.1010 COD+3.7706	0.998	ΔI=0.1049 COD+4.9563	0.988	ΔI=0.1177 COD+5.8384	0.974
PDA	ΔI=0.0202 COD+0.4853	0.969	ΔI=0.0649 COD+0.5641	0.973	ΔI=0.0844 COD+1.9301	0.996
NaAc	ΔI=0.0772 COD+2.5856	0.988	ΔI=0.0837 COD+4.9956	0.997	ΔI=0.1263 COD+7.6423	0.992
KHP	ΔI=0.0645 COD+3.1497	0.996	ΔI=0.2309 COD+8.2145	0.998	ΔI=0.4603 COD+14.9617	0.995
MB	ΔI=0.0885 COD+4.0875	0.994	ΔI=0.4281 COD+10.905	0.995	ΔI=0.8421 COD+28.0631	0.994
MO	ΔI=0.0619 COD+0.4191	0.992	ΔI=0.1512 COD+6.4967	0.994	ΔI=0.2213 COD+10.4567	0.996
GLc	ΔI=0.0274 COD+0.2554	0.994	ΔI=0.0529 COD+8.1001	0.991	ΔI=0.1188 COD+8.9911	0.981

Voltage (V·vs. SCE)	3.0		3.5	
	Linear regression equation (ΔI, μA; COD, mg/L)	R^2	Linear regression equation (ΔI, μA; COD, mg/L)	R^2
PhOH	ΔI =0.1336 COD+6.9763	0.997	ΔI=0.2148 COD+6.8624	0.992
PDA	ΔI =0.1684 COD+1.5619	0.994	ΔI=0.1945 COD+3.2386	0.984
NaAc	ΔI =0.1785 COD+9.2659	0.991	ΔI=0.2699 COD+11.9135	0.992
KHP	ΔI =0.7987 COD+31.6747	0.996	ΔI=1.3338 COD+55.7747	0.991
MB	ΔI =1.5623 COD+47.102	0.992	ΔI=2.6093 COD+94.942	0.995
MO	ΔI =0.4113 COD+22.656	0.993	ΔI=0.6763 COD+23.957	0.989
GLc	ΔI =0.2038 COD+18.491	0.991	ΔI=0.2738 COD+25.691	0.994

The PhOH, PDA, NaAc, KHP, MB, MO, and GLc represent phenol, propanedioic acid, sodium acetate, potassium hydrogen phthalate, methylene blue, methyl orange, and glucose, respectively.

As the voltage increase, the electrocatalytic effect of the used Al/SnO_2-TiO_2 electrode was significantly improved to degrade organic matter and produce electrons through the electrode reaction, thereby affecting the current [1, 50, 58-61]. Moreover, Table 1 lists the linear regression equations of COD and ΔI of the seven target organic solutions under different voltages. It demonstrated the regression equation of each organic solution was different, and the high correlation coefficient R^2 reflected the high degree of correlation between the two variables of COD and ΔI.

3.5.2 COD determination of two-component solution

To further determine the relationship of COD vs. ΔI, the current was detected in the three-

electrode system under different voltages for two-component solutions with a COD concentration gradient of 20~100 mg/L. Two kinds of organic matters were mixed in a COD ratio of 1:1 to prepare the two-component solutions of An/RhB, KHP/PhOH, NaAc/GLc, and MB/MO [62, 63].

Figure 8 shows the relationship between COD and △I for the two-component solutions at 1.5V, 2.0V, 2.5V, 3.0V, and 3.5V. The changing trend of each two-component solution was very stable and consistent with that of single-component organic solutions. The net current value of each mixed solution linearly increased with the increase of COD value in the range of 20~100 mg/L. The figure also shows that the overall net current value increased with the voltage increase. The net current was different for the different two-component organic solutions with the same COD concentration. Table 2 shows the linear regression equations of COD and △I of the two-component mixed organic solutions under different voltages. The regression equation of each organic solution was different and had a good linear relationship (R^2>0.98). Therefore, the results re-showed that the net current was affected by COD, voltage, and the type of the organic pollutant. It was attributed that the molecular structure of the target organic matter can affect the generation of electrons, thereby affecting the current [57, 64-66].

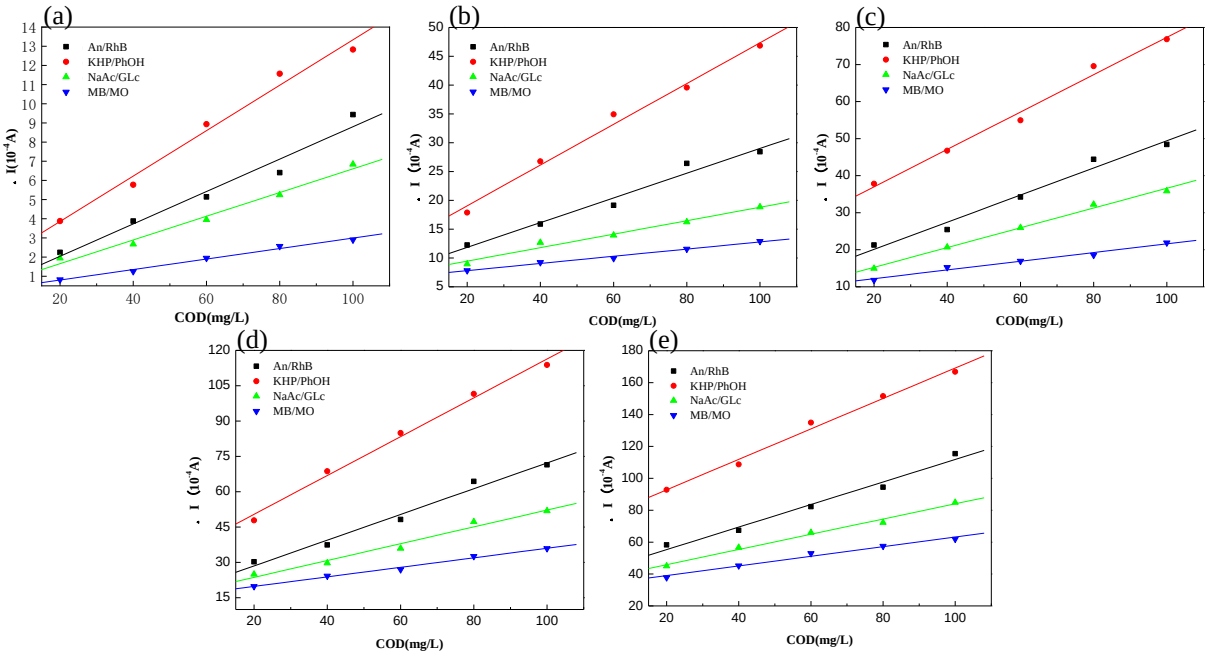

Figure 8. The linear curves of ΔI and COD of the two-component mixed solutions of An/RhB, KHP/PhOH, NaAc/GLc, and MB/MO in the COD ratio of 1:1 at the voltages of 1.5 V (a), 2.0 V (b), 2.5 V (c), 3.0 V (d), and 3.5 V (e). An, RhB, KHP, PhOH, NaAc, GLc, MB, and MO represent aniline, rhodamine B, potassium hydrogen phthalate, phenol, sodium acetate, glucose, methylene blue, and methyl orange, respectively.

Table 3. Linear regression equations of net current ΔI and COD value of the two-component solutions of An/RhB, KHP/PhOH, NaAc/GLc, and MB/MO.

Voltage (V·vs. SCE)	1.5		2.0		2.5	
	Linear regression equation	R^2	Linear regression equation	R^2	Linear regression equation (ΔI, μA;	R^2

	(ΔI, μA; COD, mg/L)		(ΔI, μA; COD, mg/L)		COD, mg/L)	
An/RhB	ΔI=0.0845 COD+0.3497	0.982	ΔI=0.2145 COD+7.5497	0.986	ΔI=0.3664 COD+12.772	0.989
KHP/PhOH	ΔI=0.0125 COD+1.4875	0.991	ΔI=0.3534 COD+11.987	0.994	ΔI=0.5044 COD+26.912	0.994
NaAc/GLc	ΔI=0.0639 COD+0.4391	0.992	ΔI=0.1169 COD+7.1191	0.989	ΔI=0.2668 COD+9.919	0.997
MB/MO	ΔI=0.0274 COD+0.2554	0.994	ΔI=0.0624 COD+6.5554	0.994	ΔI=0.1174 COD+9.854	0.989

Voltage (V·vs. SCE)	3.0		3.5	
	Linear regression equation (ΔI, μA; COD, mg/L)	R^2	Linear regression equation (ΔI, μA; COD, mg/L)	R^2
An/RhB	ΔI=0.5464 COD+17.572	0.991	ΔI=0.7064 COD+41.1717	0.991
KHP/PhOH	ΔI=0.8243 COD+33.912	0.996	ΔI=0.9544 COD+73.712	0.995
NaAc/GLc	ΔI=0.3569 COD+16.519	0.989	ΔI=0.4769 COD+36.319	0.995
MB/MO	ΔI=0.2024 COD+15.755	0.995	ΔI=0.3024 COD+32.965	0.990

An, RhB, KHP, PhOH, NaAc, GLc, MB, and MO represent aniline, rhodamine B, potassium hydrogen phthalate, phenol, sodium acetate, glucose, methylene blue, and methyl orange, respectively.

3.5.3 COD determination of three-component solution

In this section, the Al/SnO_2-TiO_2 electrode was used to measure the COD of three-component mixed solutions. The COD ratio of the measured organic matters was 1:1:1 in the three-component solution. At the voltages of 1.5 V, 2.0 V, 2.5 V, 3.0 V, and 3.5 V (vs. SCE), the current variation values of the three-component organic solutions in the COD range of 20~100 mg/L were measured by chronocoulometry and shown in Figure 9. With the increase of COD value, △I value increased. The current ranged from 1.1~1.8 μA to 91.1~236.1 μA at the operating voltages from 1.5 V to 3.5 V. The current variation range was maximum at 3.5 V, which meant that the net current increased most rapidly compared with the results at other voltages. It was attributed to the increase of the direct oxidation and the generation of more hydroxyl radicals (·OH) which improved the efficiency of indirect oxidation and increased the net current [1, 50, 58, 67, 68]. In addition, the figure shows that the net current value of the An/NaAc/GLc solution was the highest, while that of the MB/PhOH/HAc solution was the lowest. It also indicated that at the same COD concentration, the oxidation current values of the mixed solutions with different types of organic substances on the Al/SnO_2-TiO_2 electrode were different. It further demonstrated the different relationships of COD vs. △I and the different catalytic degradation capabilities of the three-component mixed solutions, owing to the different functional groups. Table 4 lists the linear regression equations of COD vs. △I for the four three-component organic solutions under different voltages. In Table 4, the regression equation of each organic solution was different and had a linear relationship (R^2>0.99). And the slope of the linear regression equation of the An/NaAc/GLc solution was the largest, compared with the other two mixed organic solutions. Therefore, within the COD range of 20~100 mg/L, the current increase rate of the An/NaAc/GLc solution was the largest due to the significant improvement of the electrocatalytic reactivity.

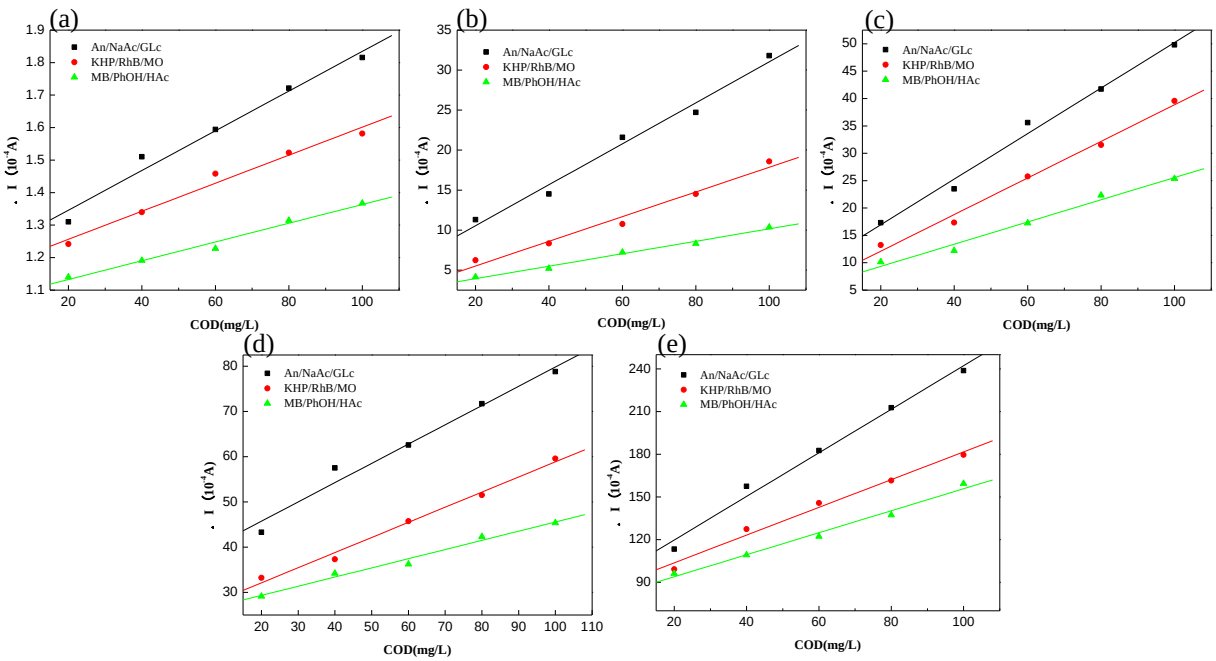

Figure 9. The linear curves of ΔI and COD of the three-component mixed solutions of An/NaAc/GLc, KHP/RhB/MO, and MB/PhOH/HAc in the COD ratio of 1:1:1 at the voltages of 1.5 V (a), 2.0 V (b), 2.5 V (c), 3.0 V (d), and 3.5 V (e). An, NaAc, GLc, KHP, RhB, MO, MB, PhOH, and HAc represent aniline, sodium acetate, glucose, potassium hydrogen phthalate, rhodamine B, methyl orange, methylene blue, phenol, and acetic acid, respectively.

Table 4. Linear regression equations of net current ΔI and COD value of the three-component mixed solutions of An/NaAc/GLc, KHP/RhB/MO, and MB/PhOH/HAc.

Voltage (V·vs. SCE)	1.5		2.0		2.5	
	Linear regression equation (ΔI, μA; COD, mg/L)	R^2	Linear regression equation (ΔI, μA; COD, mg/L)	R^2	Linear regression equation (ΔI, μA; COD, mg/L)	R^2
An/NaAc/GLc	ΔI=0.0061 COD+1.2237	0.988	ΔI=0.2561 COD+5.4237	0.991	ΔI=0.4161 COD+8.6237	0.994
KHP/RhB/MO	ΔI=0.0043 COD+1.1701	0.989	ΔI=0.1543 COD+2.4307	0.989	ΔI=0.3343 COD+5.4301	0.995
MB/PhOH/HAc	ΔI=0.0029 COD+1.0749	0.992	ΔI=0.0779 COD+2.3749	0.994	ΔI=0.2029 COD+5.2749	0.995
Voltage (V·vs. SCE)	3.0		3.5			
	Linear regression equation (ΔI, μA; COD, mg/L)	R^2	Linear regression equation (ΔI, μA; COD, mg/L)	R^2		
An/NaAc/GLc	ΔI=0.4261 COD+37.223	0.988	ΔI=1.5310 COD+89.124	0.994		
KHP/RhB/MO	ΔI=0.3343 COD+25.431	0.995	ΔI=0.9743 COD+84.231	0.993		
MB/PhOH/HAc	ΔI=0.2028 COD+25.274	0.991	ΔI=0.7729 COD+78.474	0.993		

An, NaAc, GLc, KHP, RhB, MO, MB, PhOH, and HAc represent aniline, sodium acetate, glucose, potassium hydrogen phthalate, rhodamine B, methyl orange, methylene blue, phenol, and acetic acid, respectively.

Thus, it re-confirmed the types of organics that affected the electrochemical process on the prepared Al/SnO_2-TiO_2 electrode surface due to their molecular structure and electrochemical reactivity.

3.5.4. Correlation analysis of COD with standard potassium dichromate method

The applicability of the COD determination was analyzed by comparing the Al/SnO_2-TiO_2 electrode method with the standard potassium dichromate method. By simulating the wastewater with potassium hydrogen phthalate, the COD concentration of the prepared solution ranged from 20 mg/L to 100 mg/L. As shown in Figure 10, there was a good correlation between the experimental COD value and the standard COD value of the solution measured by the two methods. In the case of a valid test range, the Pearson correlation coefficient [61] was used as a measure of the correlation strength between the COD values obtained from the electrochemical (COD_{EC}) method and the standard (COD_{Cr}) method [69]. The linear equation obtained by fitting was y=0.445+1.0334x, r=0.994, indicating a high degree of consistency between the two methods. The almost identical slope value indicated that both of the methods could accurately measure the COD value. The applicability of the electrochemical method for measuring COD was strongly supported by the high correlation and the identical slopes.

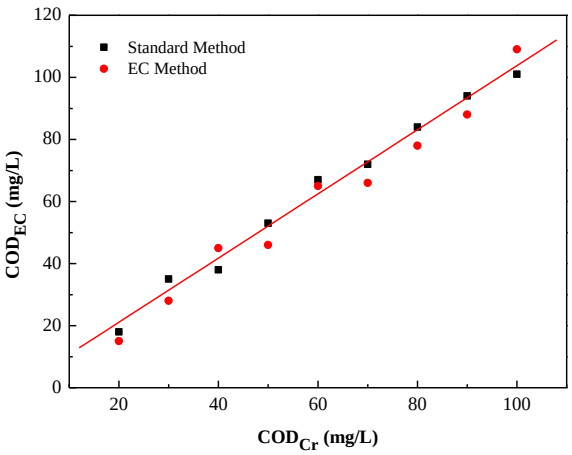

Figure 10. The correlation between the Al/SnO_2-TiO_2 composite electrode electrochemical (COD_{EC}) method and the standard potassium dichromate (COD_{Cr}) method for COD measurement.

Table 5 shows the comparison of the recently developed electrodes containing TiO_2 for COD determination in previously reported literature and summarizes the electrode preparation method, target organic substance, operation time, etc. In Table 5, it can be found that some research mentioned the detection of the multi-component solution, but the study for the type of organic matter was limited [70, 71]. However, more extensive research is of great importance for an actual COD determination. This work achieved a complete and comprehensive study on electrochemical determination of COD, especially for the measurement of more single-component and multi-component solutions. The preparation method of the Al/SnO_2-TiO_2 electrode is easy, fast, and beneficial to mass production without

any complicated operations or expensive instruments, compared to the others in Table 5. The COD determination using the prepared electrode in this work took a shorter operation time than other detection listed in the table. Future research should include the development of electrode preparation, the study of influence factors of electrocatalytic degradation of organic solutions on the electrode, etc., to in-deep research and improve the electrochemical method for COD determination.

Table 5. Comparison of the electrodes containing TiO_2 for COD determination in previously reported literature

Detection method	Electrode	Preparation method	Linearity range (mg/L)	Target organic substance	Operation time (s)	Reference
PEC	Ti/TiO_2 photoelectrode	Laser Anneal	50~2000	S: KHP	>30	[4]
PEC using flow injection	Ti/TiO_2 photoelectrode	Laser Anneal	5~1000	S: KHP	>100	[72]
PEC	Ti/TiO_2/PbO_2 photoelectrode	Dip-coating combined with laser anneal	20~2500	S: KHP	>30	[73]
PEC	Mixed-phase TiO_2 electrode	Dip-coating	0~200	S: KHP, GLc, GrA, SuA, PDA; M: GLc/GtA	-	[70]
EC	Ti/Sb–SnO_2/PbO_2 composite electrode	Electrochemical deposition	0.5~200	S: GLc, Su, Np, HQ, p-HbA, Te	>30	[16]
EC	Ti/TiO_2 electrode	Anodic oxidation	20~2500	S: KHP	100	[2]
EC	Ti/TiO_2 nanotube array electrode	Secondary anodic oxidation	5~150	S: An, RhB, KHP; M: An/KHP, An/RhB, RhB/KHP, An/RhB/KHP	60	[71]
EC	Al/SnO_2-TiO_2 composite film electrode	Sol-gel method combined with dip-coating	20~100	S: PhOH, PDA, NaAc, KHP, MB, MO, GLc, M: An/RhB, KHP/PhOH, NaAc/GLc, MB/MO, An/NaAc/GLc, KHP/RhB/MO, MB/PhOH/HAc	20	This work

PEC represents photoelectrocatalysis and EC represents electrochemical catalysis. S and M stand for single- and multi-component organic solutions, respectively. In addition, KHP represents potassium hydrogen phthalate, and the similar representative names include An – aniline, GLc – glucose, GrA – glutaric acid, HQ – hydroquinone, MB – methylene blue, MO – methyl orange, NaAc – sodium acetate, Np –nitrophenol, PDA – propanedioic acid, p-HbA – p-hydroxybenzoic acid, PhOH – phenol, RhB – rhodamine B, Su – sucrose, SuA – succinic acid, Te – tetracycline.

In summary, in the COD range of 20~100 mg/L, the net current values of seven single-component, four two-component, and three three-component organic solutions were measured by the three-electrode chronocoulometry under different voltages. The linear regression equations between $\triangle I$ and COD were obtained with high correlation coefficients R^2. In the COD range of 20~100 mg/L, the COD value was proportional to the anodic oxidation current $\triangle I$. At the same COD concentration, the oxidation current of the different organic solutions was different, which proved that the catalytic current was related to the type of organic solution. In addition, the linear relationship between $\triangle I$ and COD was different for

different kinds of organic solutions under the same conditions, indicating that the electrocatalytic kinetics of organic substances on the Al/SnO_2-TiO_2 composite electrode surface was different [59]. As the voltage increased, the catalytic current increased. It indicated that the increase in voltage promoted generating more free radicals(·OH) and improved the catalytic efficiency [57, 64, 65]. In addition, the Al/SnO_2-TiO_2 composite electrode test system had good reproducibility and stability through the relative standard deviation analysis of the verification results through repeated experiments of simulated wastewater with potassium hydrogen phthalate. The electrochemical method using the Al/SnO_2-TiO_2 composite electrode was compared with the standard COD method (potassium dichromate method). The high correlation and the identical slopes indicated a high degree of consistency between both measured COD values, demonstrating that both approaches could accurately measure the same COD value[60].

4. CONCLUSION

The Al/SnO_2-TiO_2 composite film electrode was successfully prepared with three SnO_2-TiO_2 layers doped 4 wt.% Sn by sol-gel method combined with dip-coating. Confirmed by SEM, the electrode had a large specific surface area due to the uneven surface. The composition of the oxide layer of the electrode surface mainly consisted of the rutile phase TiO_2 and the cassiterite phase SnO_2. The electrocatalytic kinetics of the electrode reaction was studied for the different organic matter (methylene blue and rhodamine B). The experimental results showed that the $\ln(C_0/C_t)$-T curve for each organic solution had a good linearity, and the correlation coefficient was above 0.99. The electrocatalytic reaction of organic compounds on the electrode surface fitted the first-order kinetics. According to the reaction rate constant k at different temperatures, the activation energies of the organic solutions (methylene blue and rhodamine B) were calculated to be 9.92 kJ/mol and 14.7 kJ/mol, respectively. It demonstrated the different dynamic behavior of the organic substances on the electrode surface. For COD determination, the net current value of the standard organic solution was measured under different voltages, among a COD concentration gradient of 20~100 mg/L. The target organic solutions in this experiment included seven single-component and seven multi-component organic solutions. The results obtaining from the COD measurement of the single-component and multi-component organic solutions were consistent. In the COD range of 20~100 mg/L, the anodic oxidation current was proportional to the COD value of the organic solution. At the same COD concentration, the oxidation current of different organic substances was different, reproving that the electrocatalytic kinetic behavior for organic substances on the electrode surface was different. Thus, in the electrocatalytic oxidation determination of COD, the oxidation current was affected by the working voltage, the COD concentration of organic matter, and the species of organic matter. Therefore, this report offered a simple, fast, and environmental-friendly way of COD determination by the Al/SnO_2-TiO_2 electrode method. The prepared composite electrode could also be applied in electrochemical degradation of water pollutions for wastewater treatment and other electrochemical processes such as an online monitor for wastewater containing organic pollutants.

References

1. Q. Zheng, B. Zhou, J. Bai, L. Li, Z. Jin, J. Zhang, J. Li, Y. Liu, W. Cai and X. Zhu, *Adv. Mater*., 20 (2008) 1044.
2. Y. Ge, Y. Zhai, D. Niu, Y. Wang, C. Fernandez, T. Ramakrishnappa, X. Hu and L. Wang, *Int. J. Electrochem. Sci.*, 11 (2016) 9812.
3. C. R. Silva, C. D. C. Conceição, V. G. Bonifácio, O. F. Filho and M. F. S. Teixeira, *J. Solid State Electrochem.*, 13 (2009) 665.
4. J. Li, L. Zheng, L. Li, G. Shi, Y. Xian and L. Jin, *Electroanaly*., 18 (2006) 1014.
5. S. Lee and -. H. K. Ahn, *Water Sci. Technol*., 50 (2004) 57.
6. S. Dong, X. Chen, X. Zhang and G. Cui, *Coord. Chem. Rev*., 257 (2013) 1946.
7. Y. Moriya, T. Takata and K. Domen, *Coord. Chem. Rev*., 257 (2013) 1957.
8. M. A. Jirka and J. M. Carter, *Anal. Chem*., 47 (1975) 1397.
9. A. Cuesta, L. J. Todoli and A. Canals, *Spectrochimica Acta Part* B 51 (1996) 1791.
10. H. Wang, Q. Guan, J. Li and T. Wang, *Catal. Today*, 236 (2014) 121.
11. J. N. Louvet, B. Homeky, M. Casellas, M. N. Pons and C. Dagot, *Chemosphere*, 91 (2013) 648.
12. N. Matsché and K. Stumwöhrer, *Water Sci. Technol*., 33 (1996) 211.
13. J. Wang, C. Wu, K. Wu, Q. Cheng and Y. Zhou, *Anal. Chim. Acta*, 736 (2012) 55.
14. R. Bogdanowicz, J. Czupryniak, M. Gnyba, J. Ryl, T. Ossowski, M. Sobaszek, E. M. Siedlecka and K. Darowicki, *Sensor. and Actuat. B-Chem*., 189 (2013) 30.
15. T. Kondo, Y. Tamura, M. Hoshino, T. Watanabe, T. Aikawa, M. Yuasa and Y. Einaga, *Anal. Chem.*, 86 (2014) 8066.
16. C. Ma, F. Tan, H. Zhao, S. Chen and X. Quan, *Sensor. and Actuat. B-Chem*., 155 (2011) 114.
17. Q. H. Nguyen, T. Watari, T. Yamaguchi, Y. Takimoto, K. Niihara, J. P. Wiff and T. Nakayama, *Int. J. Electrochem. Sci.*, 15 (2020) 39.
18. O. M. Pacheco-Álvarez, M. O. Rodríguez-Narváez, K. Wrobel, R. Navarro-Mendoza, L. J. Nava-Montes de Oca and M. J. Peralta-Hernández, *Int. J. Electrochem. Sci*., 13 (2018) 11549.
19. Q. Chen, *Int. J. Electrochem. Sci*., (2018) 7301.
20. Q. H. Nguyen, Y. Kawamura, T. Watari, K. Niihara, T. Yamaguchi and T. Nakayama, *Int. J. Electrochem. Sci*., 15 (2020) 493.
21. H. Zhu, *Int. J. Electrochem. Sci*., (2021) ArticleID:210526.
22. H. Yu, H. Wang, X. Quan, S. Chen and Y. Zhang, *Electrochem. Commun*., 9 (2007) 2280.
23. Y. Zhou, T. Jing, Q. Hao, Y. Zhou and S. Mei, *Electrochim. Acta*, 74 (2012) 165.
24. Q. Mu, Y. Li, Q. Zhang and H. Wang, *Sensor. and Actuat. B-Chem*., 155 (2011) 804.
25. A. Zhang, M. Zhou and Q. Zhou, *Anal. Chim. Acta*, 686 (2011) 133.
26. S. Li, F. Zheng, S. Cai, W. Liang and Y. Li, *Sensors and Actuators* B 188 (2013) 280.
27. C. Li and G. Song, *Sensor. and Actuat. B-Chem*., 137 (2009) 432.
28. Z. Zhang, Y. Yuan, Y. Fang, L. Liang, H. Ding and L. Jin, *Talanta*, 73 (2007) 523.
29. J. Li, L. Li, L. Zheng, Y. Xian and L. Jin, *Talanta*, 68 (2006) 765.
30. T. Carchi, B. Lapo, J. Alvarado, P. J. Espinoza-Montero, J. Llorca and L. Fernandez, *Sensors*, 19 (2019) 1.
31. S. Ai, M. Gao, Y. Yang, J. Li and L. Jin, *Electroanaly*., 16 (2004) 404.
32. H. Mo, Y. Tang, X. Wang, J. Liu, D. Kong, Y. Chen, P. Wan, H. Cheng, T. Sun, L. Zhang, M. Zhang, S. Liu, Y. Sun, N. Wang, L. Xing, L. Wang, Y. Jiang, X. Xu, Y. Zhang and X. Meng, *Electrochim. Acta*, 176 (2015) 1100.
33. N. Abdessamad, H. Akrout and L. Bousselmi, *Environ. Technol*., 36 (2015) 3201.
34. Z. Yi, Y. Zeng, H. Wu, X. Chen, Y. Fan, H. Yang, Y. Tang, Y. Yi, J. Wang and P. Wu, *Results Phys*., 15 (2019) 102609.
35. H. Cheshideh and F. Nasirpouri, *J. Electroanal. Chem*., 797 (2017) 121.
36. S. Ramasundaram, M. G. Seid, W. Lee, C. U. Kim, E. J. Kim, S. W. Hong and K. J. Choi, *J.*

Hazard. Mater., 340 (2017) 300.
37. S. Chen, L. Zhou, T. Yang, Q. He, P. Zhou, P. He, F. Dong, H. Zhang and B. Jia, *Chemosphere*, 261 (2020) 128201.
38. M. Song, H. Cao, Y. Zhu, Y. Wang, S. Zhao, C. Huang, C. Zhang and X. He, *Chem. Phys. Lett*., 747 (2020) 137355.
39. L.-C. Chen, F.-R. Tsai, S.-H. Fang and Y.-C. Ho, *Electrochim. Acta*, 54 (2009) 1304.
40. Z.-x. Fan, Y.-c. Sun and J.-l. Chen, *Chinese Journal of Semiconductors*, 22 (2001) 1382.
41. Y. Zhang, P. He, L. Zhou, F. Dong, D. Yang, H. Lei, L. Du, L. Jia and S. Zhou, *Ecotoxicol. Environ. Saf*., 188 (2020) 109921.
42. S. Chen, J. Li, L. Liu, Q. He, L. Zhou, T. Yang, X. Wang, P. He, H. Zhang and B. Jia, *Chemosphere*, 256 (2020) 127139.
43. Y. Liu, B. Zhou, J. Bai, J. Li, J. Zhang, Q. Zheng, X. Zhu and W. Cai, *Appl. Catal. B-Environ*., 89 (2009) 142.
44. M. Zhou, J. Yu, S. Liu, P. Zhai and L. Jiang, *J. Hazard. Mater*., 154 (2008) 1141.
45. R. Daghrir, P. Drogui, I. Ka and M. A. El Khakani, *J. Hazard. Mater*., 199-200 (2012) 15.
46. R. Daghrir, P. Drogui, A. Dimboukou-Mpira and M. A. El Khakani, *Chemosphere*, 93 (2013) 2756.
47. S. Millesi, R. Lo Nigro, M. Pedroni, A. Speghini and A. Gulino, *J. Phys. Chem*. B, 119 (2015) 23743.
48. C. A. Martínez-Huitle, M. A. Rodrigo, I. Sirés and O. Scialdone, *Chem. Rev*., 115 (2015) 13362.
49. Q. Dai, L. Jiang and X. Luo, *Int. J. Electrochem. Sci*., 12 (2017) 4265.
50. Z. Chen, G. Xie, Z. Pan, X. Zhou, W. Lai, L. Zheng and Y. Xu, *J. Alloys Compd*., 851 (2021) 156834.
51. S. Garcia-Segura, J. D. Ocon and M. N. Chong, *Process Saf. Environ*., 113 (2018) 48.
52. C. Shao, F. Zhang, X. Li, J. Zhang, Y. Jiang, H. Cheng and K. Zhu, *J. Electroanal. Chem*., 832 (2019) 436.
53. M. Zhou, Z. Wu and D. Wang, *J. Environ. Sci. Health., Part* A, 37 (2007) 1263.
54. R. Mei, C. Zhu, Q. Wei, L. Ma, W. Li, B. Zhou, Z. Deng, Z. Tong, G. Ouyang and C. Jiang, *J. Electrochem. Soc*., 165 (2018) H324.
55. I. C. da Costa Soares, D. R. da Silva, J. H. O. do Nascimento, S. Garcia-Segura and C. A. Martínez-Huitle, *Environmental Science and Pollution Research*, 24 (2017) 24167.
56. W. Chen, W. Li, F. Liu, D. Miao, L. Ma, X. Gao, Q. Wei, K. Zhou, Z. Yu and Y. Yu, *Journal of Environmental Chemical Engineering*, 8 (2020) 104348.
57. T. Xu, J. Song, W. Lin, B. Fu, X. Guo, X. Huang, H. Wu and X. Zhang, *Appl. Energ*., 281 (2021) 115913.
58. P. Saha, H. Bruning, T. V. Wagner and H. H. M. Rijnaarts, *Chemosphere*, 259 (2020) 127491.
59. G. S. Yan and T. J. Hupp, *The Journal of Physical Chemistry*, 100 (1996) 6867.
60. C. Wang, J. Wu, P. Wang, Y. Ao, J. Hou and J. Qian, *Sensor. and Actuat. B-Chem*., 181 (2013) 1.
61. B. Qiu, Y. Zhou, Y. Ma, X. Yang, W. Sheng, M. Xing and J. Zhang, *Scientific Reports*, 5 (2015) 1.
62. H. Xu, A. Li and X. Cheng, *Int. J. Electrochem. Sci*., 6 (2011) 5114.
63. T. Zayas, M. Picazo, U. Morales, E. Torres and L. Salgado, *Int. J. Electrochem. Sci.*, 10 (2015) 7840.
64. M. Chen, S. Pan, C. Zhang, C. Wang, W. Zhang, Z. Chen, X. Zhao and Y. Zhao, *Chem. Eng. J*., 399 (2020) 125756.
65. D. Yu, X. Zhu, Z. Xu, X. Zhong, Q. Gui, Y. Song, S. Zhang, X. Chen and D. Li, *ACS Appl. Mater. Inter.*, 6 (2014) 8001.
66. V. Vaiano, D. Sannino and O. Sacco, Chapter 9 - The use of nanocatalysts (and nanoparticles) for water and wastewater treatment by means of advanced oxidation processes, in Nanotechnology in the Beverage Industry, A. Amrane, et al., Editors. 2020, Elsevier. p. 241.
67. Z. Cao, D. Wen, H. Chen and J. Wang, *Int. J. Electrochem. Sci*., 11 (2016) 4018.
68. M. Jović, D. Stanković, D. Manojlović, I. Anđelković, A. Milić, B. Dojčinović and G. Roglić, *Int.*

J. Electrochem. Sci., 8 (2013) 168
69. H. Zhang, Z. Xu, S. Wang and X. Fan, *Int. J. Electrochem. Sci*., 15 (2020) 12462.
70. S. Zhang, L. Li and H. Zhao, *Environ. Sci. Technol*., 43 (2009) 7810.
71. X. Li, L. Wang and L. Wang, *Water Sci. Technol*., (2021).
72. J. Li, L. Zheng, L. Li, G. Shi, Y. Xian and L. Jin, *Meas. Sci. Technol*., 18 (2007) 945.
73. J. Li, L. Zheng, L. Li, G. Shi, Y. Xian and L. Jin, *Electroanalysis*., 18 (2006) 2251